NMR relaxation studies in doped poly-3-methylthiophene

K. Jugeshwar Singh,[1,*] W. G. Clark,[2] G. Gaidos,[2] A. P. Reyes,[3] P. Kuhns,[3] J. D. Thompson,[4] R. Menon,[1] and K. P. Ramesh[1,†]

[1]*Department of Physics, Indian Institute of Science, Bangalore-560012, India*

[2]*Department of Physics and Astronomy, UCLA, Los Angeles, California 90095-1547, USA*

[3]*National High Magnetic Field Laboratory, Tallahassee, Florida 32310, USA*

[4]*Los Alamos National Laboratory, Los Alamos, New Mexico 87545, USA*

(Received 9 December 2014; revised manuscript received 27 April 2015; published 19 May 2015)

NMR relaxation rates ($1/T_1$), magnetic susceptibility, and electrical conductivity studies in doped poly-3-methylthiophene are reported in this paper. The magnetic susceptibility data show the contributions from both Pauli and Curie spins, with the size of the Pauli term depending strongly on the doping level. Proton and fluorine NMR relaxation rates have been studied as a function of temperature (3–300 K) and field (for protons at 0.9, 9.0, 16.4, and 23.4 T, and for fluorine at 9.0 T). The temperature dependence of T_1 is classified into three regimes: (a) For $T < (g\mu_B\mathbf{B}/\mathbf{2k_B})$, the relaxation mechanism follows a modified Korringa relation due to electron-electron interactions and disorder. ^{1}H$-T_1$ is due to the electron-nuclear dipolar interaction in addition to the contact term. (b) For the intermediate temperature range $(g\mu_B\mathbf{B}/\mathbf{2k_B}) < T < T_{\mathrm{BPP}}$ (the temperature where the contribution from the reorientation motion to the T_1 is insignificant) the relaxation mechanism is via spin diffusion to the paramagnetic centers. (c) In the high-temperature regime and at low Larmor frequency the relaxation follows the modified Bloembergen, Purcell, and Pound model. T_1 data analysis has been carried out in light of these models depending upon the temperature and frequency range of study. Fluorine relaxation data have been analyzed and attributed to the PF_6 reorientation. The cross relaxation among the ^{1}H and ^{19}F nuclei has been observed in the entire temperature range suggesting the role of magnetic dipolar interaction modulated by the reorientation of the symmetric molecular subgroups. The data analysis shows that the enhancement in the Korringa ratio is greater in a less conducting sample. Intra- and interchain hopping of charge carriers is found to be a dominant relaxation mechanism at low temperature. Frequency dependence of T_1^{-1} on temperature shows that at low temperature $[T < (g\mu_B\mathbf{B}/\mathbf{2k_B})]$ the system shows three dimensions and changes to quasi one dimension at high temperature. Moreover, a good correlation between electrical conductivity, magnetic susceptibility, and NMR T_1 data has been observed.

DOI: 10.1103/PhysRevB.91.174421 PACS number(s): 73.61.Ph, 76.60.−k

I. INTRODUCTION

Conducting polymers in general have attracted a great deal of interest for the past three decades due to fundamental scientific reasons and also for the development of new materials for modern technology. Despite these properties, certain basic questions concerning their electronic structure, nature of the charge carriers, and the dimensionality of the charge transport are still under debate. Poly 3-alkylthiophenes are an unusual class of polymers among many other conjugated polymers due to their conductivity, processability, environmental stability, etc.

Solid-state nuclear magnetic resonance (NMR) is very sensitive tool to study the microscopic details of charge and spin distributions and their dynamics, through Knight shifts and relaxation behavior. These studies along with susceptibility and charge transport give a comprehensive insight into the conducting polymer.

Nuclear magnetic resonance spin lattice relaxation rate (T_1^{-1}) studies have been widely used to investigate the charge transport mechanism in both conventional [1] and novel organic [2], polymeric [3], and ceramic conductors [4,5]. In the usual metals, the delocalized charge carriers dominate the relaxation mechanism via the carrier dynamics due to the hyperfine interactions, whereas in disordered systems such as glasses the reorientation of the symmetric molecular groups is the main relaxation mechanism (at high temperatures), while at very low temperatures (T) the role of a two-level system is also observed [6–8]. The relaxation phenomena in several systems follow a universal behavior like many other properties; e.g., linear dependence of specific heat with temperature and quadratic variation of thermal conductivity up to a few Kelvin are explained on the basis of the phenomenological model proposed by Anderson [9] and Phillips [10] which is commonly known as a two-level system.

The well-known Korringa relaxation mechanism [11], which occurs over a wide range of T in conventional metals, is due to the s-contact hyperfine interaction, which couples the nuclear spins with the conduction electrons. It results in a linear relation between T_1^{-1} and T that is independent of the magnetic field (magnitude B). The result is often expressed as the Korringa relation $K_r = 1/(\kappa^2 T_1 T)$, where $K_r = \frac{4\pi k_B}{\hbar}(\frac{\gamma_e^2}{\gamma_n^2})$ is the Korringa constant, κ is the Knight shift, k_B is the Boltzmann constant, $\hbar$ is the Planck constant, and γ_e and γ_n are, respectively the conduction electron and nuclear gyromagnetic ratios. A deviation from this value of κ is often attributed to the contributions from electron-electron interactions (EEIs). Also when $K_r < 1$, the Stoner enhancement due to the uniform susceptibility can alter the value of κ [12]. Hence the correction to the susceptibility due to disorder, which in turn affects the Korringa ratio, has to be considered in the data analysis. For example, in Si:P the measured $(T_1T)^{-1}$ values are nearly three orders of magnitude larger than the free-electron values [12].

*jshwar@physics.iisc.ernet.in

†kpramesh@physics.iisc.ernet.in

It is important to note that both the Stoner enhancement and disorder contribute to this variation in the Korringa ratio. Also, a change in the correlation time (τ_e) for the electronic motion with temperature and a broad distribution in τ_e from sample inhomogeneities and other sources can generate a dependence of the conduction electron contribution to $(T_1T)^{-1}$ on both $\boldsymbol{B}$ and temperature which deviates strongly from the Korringa relation model.

These results suggest that it is quite important to know how disorder and EEI modify the Korringa relation in various systems. In this context conducting polymers are useful candidates since the carrier density and disorder can be varied substantially. Furthermore the intrinsic quasi one dimension (q1D) also makes it rather interesting to investigate how these factors come into play in the relaxation mechanisms. The earlier relaxation studies in conducting polymers such as polypyrrole [13], polyacetylene [14], and polyaniline [15], and organic conducting salts such as TTF-TCNQ [16], fluoroanthene $_2(PF_6)$ [17], $(pyrene)_{12}(SbF_6)_7$ [18], etc., have shown that the main relaxation mechanisms are (1) dipolar interaction between electron and nucleus, and dipolar interaction between homonuclear spins and heteronuclear spins, other than the contact term and heteronuclear spins; (2) interaction of the nuclei with conduction electrons (mobile paramagnetic centers) and with the localized, fixed paramagnetic centers.

In this work, T_1^{-1} measurements over a wide range of T and B in poly 3-methylthiophene (p3MT) doped with hexafluorophosphate (PF_6) are reported, along with measurements of conductivity, $\sigma(B = 0, 77\,\mathrm{K} < T < 300\,\mathrm{K})$, and the magnetic susceptibility (χ, $B = 0.1\,\mathrm{T}$, $3.5\,\mathrm{K} < T < 350\,\mathrm{K}$). The doping level has been varied to tune the conductivity values: in a fully doped sample (p3MT-1) $\sigma \sim 120$ S/cm and in a dedoped sample (p3MT-2) $\sigma \sim 5$ S/cm; this facilitates to investigate the role of carrier density and EEI in the NMR relaxation mechanisms. A correlation between electrical conductivity, magnetic susceptibility, and relaxation mechanisms has been observed in these samples. The results are analyzed using the modified Korringa relation in the appropriate temperature region, and the deviations are found to be more significant in the less conducting sample. Moreover, it has been observed that the proton spin lattice relaxation data give insight into the dimensionality of the sample and hence with the support of $^{19}F - T_1$, the corresponding role of both interchain and intrachain diffusion mechanisms has been suggested.

II. EXPERIMENTAL DETAILS

Conducting p3MT films, doped with PF_6, are prepared by low-temperature electrochemical polymerization at -30°C [19]. A 50 mM stoichiometric solution of monomer (3-methyl thiophene), salt (tetrabutylammonium hexafluorophosphate, $TBAPF_6$), and solvent (propylene carbonate) is made. A cylindrical cell containing electrodes made of highly polished glassy carbon (GC) (used as a working electrode or cathode) and stainless steel [used as a counterelectrode or anode] is used to carry out the polymerization. The two electrodes are separated approximately by 6 mm. Before the reaction starts, the solution is ultrasonicated for about 3 min and then bubbled for about 30 min vigorously by N_2 gas to drive away traces of oxygen from the solution. An inert atmosphere is maintained

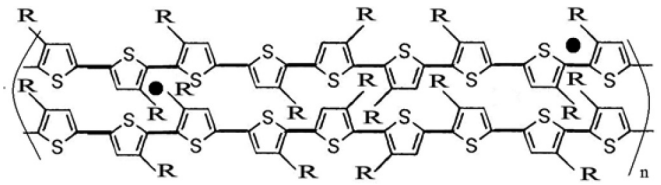

FIG. 1. Schematic diagram of the p3MT polymer with the dopants, where $R = CH_3$, the methyl side group attached to the thiophene ring, and • is PF_6, the dopant.

during the experiment. A constant current of $1\,\mathrm{mA/cm^2}$ for 30 min is applied to the electrodes. A free-standing film of 45 mm × 45 mm having a thickness of 45 μm is formed on the GC electrode at the end of the experiment. A part of the film is peeled off for analysis (considered as highly doped, named p3MT-1). In the remaining part of the sample (lightly doped, named p3MT-2), a reversed current of $0.5\,\mathrm{mA/m^2}$ is applied for 20 min to the electrodes. This process of applying reverse current is called dedoping. During the reversed current the PF_6 ions are removed from the prepared polymer system. Both the highly doped (p3MT-1) and lightly doped (p3MT-2) samples are used for conductivity, susceptibility, and NMR studies. Since the dopants are intercalated between the polymer chains, the structure of the p3MT chains with dopants looks as depicted in the schematic diagram in Fig. 1 [20].

Measurements of σ as a function of T were made using the standard four-probe technique using a dipstick. The variations of σ as a function of T for p3MT-1 and p3MT-2 are shown in Fig. 2.

Magnetic susceptibility measurements are carried out using a Quantum Design SQUID magnetometer between 3.5 and 350 K at 0.1 T. SQUID measurements of χ for p3MT-1 and p3MT-2 as a function of T (3.5–350 K) are shown in Fig. 3. Since the conductivity of the p3MT-2 sample goes down by nearly two orders of magnitude, from 300 to 77 K, it typically shows the activated transport observed in semiconducting systems, so the relaxation studies are carried out only in a limited range of temperature and magnetic field. Meanwhile the charge carrier density in the p3MT-1 sample is close to that in metallic systems; as indicated from the magnetic

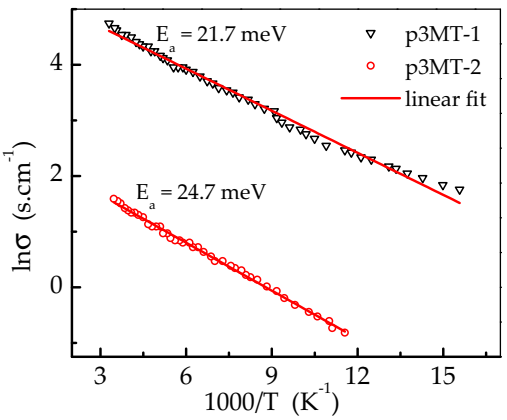

FIG. 2. (Color online) Temperature (T) dependence of conductivity (σ) for p3MT-1 (▽) and p3MT-2 (○).

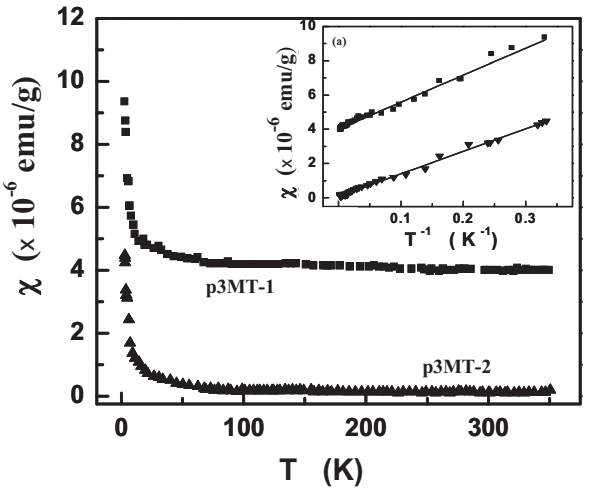

FIG. 3. Temperature dependence of susceptibility for p3MT-1 (■) and p3MT-2 (▲) at 0.1 T. Inset: Susceptibility as a function of T^{-1}; solid line is fit to Eq. (1).

susceptibility data, the detailed high magnetic field ^{1}H-T_1 measurements were done only in this sample. Measurements of T_1^{-1} as a function of T for ^{1}H and ^{19}F in both samples are shown in Fig. 4. There are two issues involved in the present NMR experiments: measurement of (i) spin lattice relaxation time and (ii) doping level in the two samples.

(a) Measurement of spin lattice relaxation time. Measurements were performed at 0.9 T by monitoring the magnetization recovery of the proton spin echo, while measurements at higher fields were conducted by monitoring the recovery of the Free Induction Decay (FID). The ^{1}H measurements in the p3MT-1 sample were done at four values of B (0.9, 9.0, 16.4, and 23.4 T) as shown in Fig. 4(a), while the p3MT-2 sample was measured only at 0.9 T. ^{19}F-T_1 measurement at 9.0 T is also done using FID signals [Fig. 4(b)].

(b) Doping level calculation. Measurement of the doping level in the two samples has been carried out at 0.9 T, by taking the ratio of the number of ^{19}F spins to that of ^{1}H spins. For this purpose, the experiment has been conducted in the following manner. The number of protons is estimated by first measuring the T_1 of the sample protons by monitoring the recovery of the free induction decay after application of a saturation train to estimate the value of T_1. Another FID was recorded after waiting for an appropriate time interval of (5 times T_1) so as to ensure the complete recovery of the magnetization. Similarly, a T_1 measurement was performed on the fluorine in each sample; only in the case of fluorine an echo was monitored to minimize spurious signal contributions. With the recovery time determined, a fully recovered fluorine FID was recorded. Then, the maximum magnitudes of the recorded FID signals were used to determine the ratio of PF_6 dopants to the single-ring monomer units of the polythiophene. The calculation assumed that the receiving coil was identically tuned and matched in the case of the two nuclei, but took into

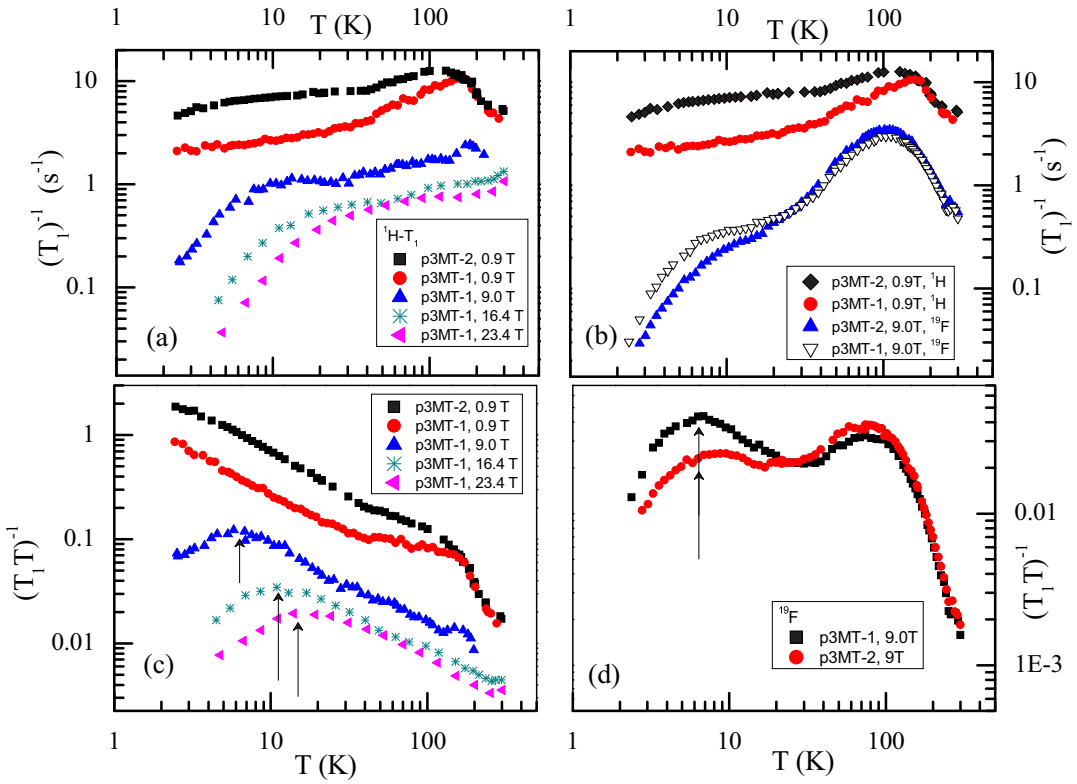

FIG. 4. (Color online) (a) ^{1}H $1/T_1$ as a function of T for p3MT-2 at 0.9 T and p3MT-1 at 0.9, 9.0, 16.4, and 23.4 T. (b) Plot of ^{19}F-T_1^{-1} as a function of T for p3MT-2 (▲) and p3MT-1 (▽) at 9 T and comparison to ^{1}H-T_1^{-1} for p3MT-2 (■) and p3MT-1 (●) at 0.9 T. (c) ^{1}H-$(T_1T)^{-1}$ as a function of T for p3MT-2 at 0.9 T and p3MT-1 at 0.9, 9.0, 16.4, and 23.4 T.(d) Plot of ^{19}F-$(T_1T)^{-1}$ as a function of T for p3MT-2(●) and p3MT-1(■) at 9 T. The vertical arrows show the value of T given by the condition $g\mu_B B = 2k_B T$.

account the relative sensitivity of the nuclei themselves, as well as the number of protons on each ring. This estimation shows that p3MT-1 has a dopant concentration of ∼0.1 per ring while p3MT-2 has ∼0.02 per ring (a monomer unit).

III. RESULTS AND DISCUSSION

A. Electrical conductivity and magnetic susceptibility

Samples p3MT-1 and p3MT-2 have room temperature conductivities of 120 and 5 S/cm, respectively. A plot of $\ln\sigma$ as a function of $1/T$ for p3MT-1 [σ (300 K) ∼ 120 S/cm)] and p3MT-2 [σ (300 K) ∼ 5 S/cm)] shown in Fig. 2, which shows a semiconducting behavior. The data at $T < 70$ K (not shown) show some scattering due to the increase in the contact resistance at lower temperatures. The fit shows a linear behavior for both the samples indicating a thermally activated transport. From the Arrhenius plot it is observed that activation energies of p3MT-1 and p3MT-2 samples are 21.7 and 24.7 meV, which are above the minimum level (∼10 meV) of thermal activation process. Moreover, both the samples are doped and thus have high charge carrier concentration of the order of 10^{20} which in turn decreases the hopping length. Thus it helps in enhancing the hopping transport process. Although σ (300 K) for p3MT-1 has the same order of magnitude as that for metallic polypyrrole (PPy) and polyaniline [21], its (σ) strong reduction with decreasing temperature suggests that a large number of carriers undergo intrachain localization at low temperature. This behavior was further investigated using measurements of susceptibility.

The susceptibility $\chi(T)$ for p3MT-1 and p3MT-2 as a function of T_1^{-1} at 0.1 T is shown in Fig. 3. Results of susceptibility vs temperature of the samples display a Fermi glass behavior [22], which is characterized by the existence of Pauli susceptibility at high temperatures, with a Curie contribution to susceptibility appearing at lower temperatures.

A good fit to the data is obtained by using a sum of Curie and Pauli susceptibility,

$$\chi = \chi_c + \chi_P, \tag{1}$$

where $\chi_c = N_c\mu_B^2/k_BT$ and $\chi_P = \mu_B^2 N(E_F)$ are, respectively, the Curie and Pauli susceptibilities, N_c is the number of Curie spins, k_B is the Boltzmann constant, $N(E_F)$ is the conduction electron density of states at Fermi energy (E_F), and μ_B is the Bohr magneton. This behavior is widely observed in several conducting polymers due to the coexistence of both Curie and Pauli spins, since the carriers tend to be localized in the amorphous regions and are delocalized in the partially crystalline domains [22–27]. The fit parameters obtained from these data are listed in Table I.

TABLE I. Parameters for σ and χ_P, $N(E_F)$, and N for p3MT-1 and p3MT-2. The susceptibility parameters are obtained from the fit to Eq. (1).

Sample	σ (∼300 K) (S/cm)	χ_P (emu/g)	$N(E_F)$ (states/eV–C)	N_c (per ring)
p3MT-1	120	4×10^{-6}	1.48	3.15×10^{13}
p3MT-2	5	0.85×10^{-7}	0.03	2.07×10^{13}

The Pauli contribution provides a direct measure of $N(E_F)$, indicating that the number of delocalized carriers in p3MT-1 is rather high. The value of $N(E_F)$ in p3MT-1 is ∼50 times larger than that of p3MT-2, while the number of Curie spins is nearly the same in both samples. These results agree with the larger value of σ (24 times larger) observed in p3MT-1. In p3MT-1, the Curie and Pauli terms are equal at around 4.2 K. These values of χ_P and $N(E_F)$ are comparable with the earlier reports in conducting polymers [28]. Thus we have seen that there is consistency between the conductivity of the samples, doping level, and $N(E_F)$.

B. Presentation of the ^{1}H and ^{19}F NMR T_1 data

In this section, we describe the important features of the ^{1}H-T_1 and ^{19}F-T_1 data as a function of the Larmor frequency (f) and temperature as shown in Figs. 4(a) and 4(b).

(1) T_1^{-1} shows a substantial dependence on both frequency and temperature, which is quite different from those observed in normal metals like Cu, etc. [1].

(2) As seen in Fig. 4(a), T_1^{-1} at 0.9 T has a maximum at T below 200 K that occurs at 182 and 165 K, respectively, for p3MT-1 and p3MT-2. Since this feature is more pronounced in the former, more detailed studies are carried out for p3MT-1 at higher magnetic fields. The data in Fig. 4(a) also show that this maximum is smeared out and shifted to higher temperature at 16.4 and 23.4 T.

(3) The ^{19}F-T_1^{-1} data for both samples at 9.0 T in Fig. 4(b) show a maximum at around 100 K. This value of temperature is significantly lower than the temperature where ^{1}H-T_1^{-1} maximum was observed at 9.0 T (∼182 K) in Fig. 4(a).

(4) Another important feature of Fig. 4 is that at 0.9 T, T_1^{-1} for ^{1}H below 150 K is less for p3MT-1 than for p3MT-2.

(5) Unlike ^{1}H-T_1, the ^{19}F relaxation rate [Fig. 4(b)] shows a crossover in relaxation rate between these two samples at $T \sim 25$ K; i.e., T_1^{-1} for ^{19}F in p3MT-1 is larger than in p3MT-2 below 25 K.

(6) To emphasize the deviation from Korringa behavior, we plot $(T_1T)^{-1}$ vs T as shown in Figs. 4(c) and 4(d). The 0.9 T data show a negative slope in $(T_1T)^{-1}$ vs T plot with increasing temperature while for the same sample at 9.0, 16.4, and 23.4 T, a similar trend is observed from 8 to 120 K, 15 to 250 K, and 20 to 250 K, respectively, while at lower temperature there is a drop in $(T_1T)^{-1}$ with decreasing temperature that occurs near 6.04 K for 9.0 T, 11.02 K for 16.4 T, and 15.72 K for 23.4 T.

Figure 4(d) shows $(T_1T)^{-1}$ as a function of temperature for ^{19}F in both samples at 9.0 T. ^{19}F-$(T_1T)^{-1}$ has two broad peaks, one around 110 K for both samples (in the form of the superposition of two peaks) and other peaks at 6.5 and 8.0 K for p3MT-1 and p3MT-2, respectively. An interpretation of these results is presented in Sec. III C 3 b.

The salient features in relaxation times are (i) change of slope in $(T_1T)^{-1}$ with T at temperature $T_z = \frac{g\mu_B \boldsymbol{B}}{2k_B}$ and (ii) the observation of a crossover of T_1 in ^{19}F.

C. Analysis of NMR T_1

The observed NMR-T_1 data for both the samples have substantial dependence not only on temperature and Larmor frequency, but they also depend on the sample conductivity. It

might obviously be due to the disorder nature of conducting polymers resulting in a wide range of electron dynamics and interactions at different values of temperature, frequency, and conductivity. To get a better insight, one can analyze the T_1 data by considering its variation with respect to (1) frequency, (2) temperature, and (3) the NMR nuclei under study.

1. *Analysis of T_1 as a function of frequency*

Before analyzing the T_1^{-1} against temperature data in the present system it is important to find out the dimensionality of the system under consideration. There are many studies [14–17,29–31] where NMR relaxation rate as a function of Larmor frequency in systems like conducting polymer and organic salts has been reported. They also reported that a plot of T_1^{-1} against frequency gives the information about the dimensionality of the system. It has been shown that the spectral density function, $f(\omega)$, reflects the electronic spin motion and depends sensitively on the dimensionality of the process. In one dimension, $f(\omega)$ is proportional to $\omega^{-1/2}$ and in two dimensions $f(\omega)$ displays a logarithmic divergence, while in three dimensions, it is nearly constant.

It is found that a majority of the T_1 studies in conducting polymers and organic salts have been carried out either at low frequency as a function of temperature or at high frequencies at room temperature only. Thus it is evident that a system can show different dimensionality depending upon the selection of temperature and frequency. Hence, with these limited experiments covered in the literature, it is difficult to draw a converging conclusion on the system dimensionality.

We have carried out a study of frequency dependence of T_1^{-1} in p3MET-1. Figure 5 shows T_1^{-1} vs frequency ($f = \omega/2\pi$) for a few representative temperatures. The frequency dependence of T_1^{-1} does not follow a similar pattern for all the temperatures studied. Dimensionality dependence of the system can also be classified from the nature of the frequency dependence of T_1^{-1} data. In the case of 3D, T_1^{-1} is independent of frequency while T_1^{-1} has a logarithmic dependence on frequency for 2D. However, for q1D, T_1^{-1} follows $f^{-1/2}$.

For the lowest temperature studied, 4.77 K, T_1^{-1} is independent of frequency except in the case of Larmor frequency 38.3 MHz [Fig. 5(a)]. The orientational degrees of freedom of localized electrons are producing a fluctuating field which has Fourier components at Larmor frequency. Below the Zeeman splitting temperature ($T_Z = \frac{g\mu_B B}{2k_B}$) at a given field, these orientational degrees of freedom cease to exist. Thus for a field, below its Zeeman splitting temperature, the spin diffusion to paramagnetic centers freezes out. In other words, conduction electrons are pinned by the applied magnetic field below its Zeeman splitting temperature. The corresponding Zeeman splitting temperatures for conduction electrons in the magnetic fields 0.9**,** 9.0**,** 16.4**,** and 23.4 T below which the conduction electrons are pinned are 0.6, 6.04, 11.02, and 15.72 K, respectively. This is consistent with experimental data [shown in Fig. 5(a)]. A temperature of 4.77 K satisfies the condition $T < T_Z$ for the frequencies corresponding to the field 9.0, 16.4, and 23.4 T but not for 0.9 T**.** This explains the deviation of T_1 for 38.3 MHz at 4.77 K. This independent behavior of T_1^{-1} with frequency suggests that the system behaves as 3D below temperatures $T < T_Z$.

We also analyzed the T_1^{-1} vs f data with respect to temperatures greater than T_Z to find the dimensionality of the system. Figures 5(b) and 5(c) show the representative fit to the 2D model (T_1^{-1} logarithmic divergence of f) and q1D model ($f^{-1/2}$ dependence of T_1^{-1}), respectively. To identify the correct dimensionality, we have plotted the R^2 for the least-squares fit for 2D and q1D in Fig. 5(d). From the figure it is observed that the higher the temperature the better is the q1D model compared to the 2D model. From the analysis at 302.2 K, where T_1^{-1} follows the best fit to $f^{-0.5}$, it is observed that the diffusion constant, $D = 1.48 \times 10^{-10}\,\mathrm{cm^2\,s^{-1}}$.

Our analysis in the present system shows that, at temperatures below T_Z, the system shows 3D behavior, while as the temperature increases the dimensionality changes over to 2D and then to q1D. This indicates that the dimensionality of the system depends on the selection of frequency and temperature, as observed in earlier studies [14,30].

2. *Temperature dependence of relaxation rate*

We consider the following relaxation mechanisms to explain the observed T_1 *Vs* temperature behavior: (1) Dipolar interaction between homo- and heteronuclei modulated by the reorientation motion of the symmetric subgroups, (2) spin diffusion to paramagnetic centers (SDPC), and (3) relaxation by the translational and spin motion of the conduction electrons. The relative magnitude of each of these mechanisms to T_1^{-1} will depend on the range of temperature. When the conduction electrons are hopping between the localization sites, both their spin orientation and translational motion can contribute to T_1^{-1}. But when we consider free conduction band electrons, only the translational motion is important for T_1^{-1}, and a Korringa type of relaxation is expected. Thus, for the sake of convenience, the T_1 analysis has been carried out in three different temperature regions where the relaxation is dominated by (a) modified Bloembergen, Purcell, and Pound (BPP) -type relaxation [32], (b) the SDPC along with modified Korringa relaxation, and (c) the "modified Korringa-like" relaxation.

In the p3MT-1 system, as different types of T_1^{-1} variation with respect to temperature are observed, we are forced to consider different types of possible NMR relaxation mechanisms depending on the temperature range. The variation in T_1^{-1} against temperature is more pronounced at low Larmor frequency (0.9 T) than higher frequencies (9.0, 16.4, and 23.4 T),which is in concurrence with the observations of Nechtschein *et al.* [14] and Mizoguchi *et al.* [15,30], that the same material behaves like q1D at high frequencies and deviates to 3D behavior at low frequencies. This is because of the spectral density due to reorientation motion of the symmetric molecular groups having finite Fourier components at lower fields than at high fields.

Thus for more detailed study, we shall consider the data at low frequency, 0.9 T, which is presented in items 2 and 4 of Sec. III B. The observation of T_1^{-1} maximum at high temperature may be due to the reorientation motion of the symmetric groups like CH_3 and PF_6 present in the system thus following the modified BPP model. Thus it is acceptable to expect a BPP-type relaxation mechanism to interpret the T_1^{-1}

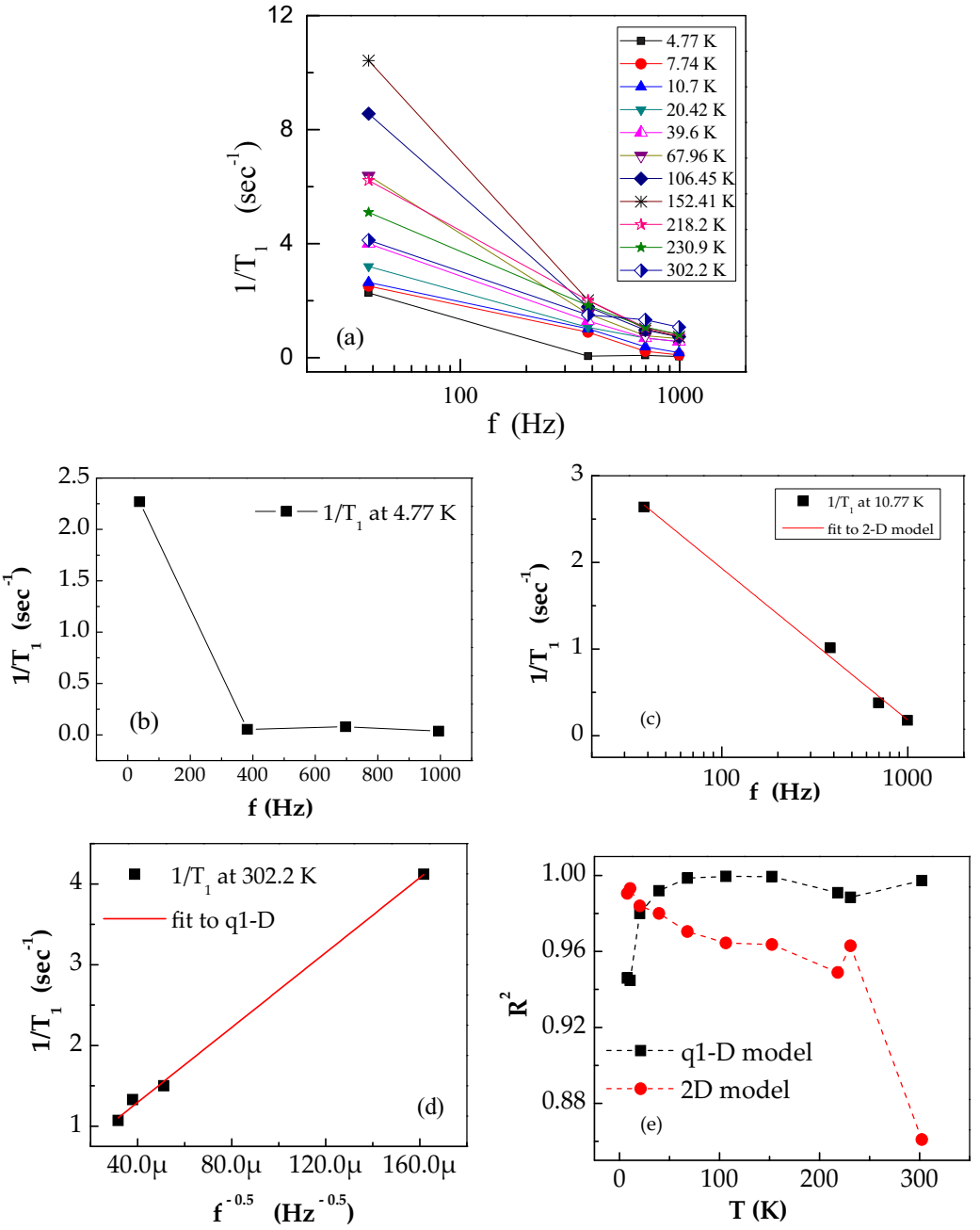

FIG. 5. (Color online) (a) ^{1}H-T_1 for p3MT-1 as a function of frequency for a few representative temperatures. Solid line is a guide to the eye. (b) ^{1}H-T_1 as a function of frequency at 4.77 K. Solid line is a guide to the eye. (c) ^{1}H-T_1 as a function of frequency at 10.7 K. Solid line is fit to the 2D model. (d) ^{1}H-T_1 as a function of frequency at 302.2 K. Solid line is fit to the q1D model. (e) R^2 for the fit to the models q1D and 2D as a function of temperature. Dashed lines are a guide to the eye.

maximum at high temperature for 0.9 T, as it gives more insight into the physics of the system.

3. *Relaxation mechanism due to reorientation motions of symmetric groups*

(a) ^{1}H-T_1 *studies.* The variation of ^{1}H-T_1 at T above 50 K is shown in Fig. 6(a) for low-field (0.9 T) data for both samples, and high-field (9 T) data for p3MT-1 are in Fig. 6(b). The data for each sample in Fig. 6(a) show a broad maximum due to the activated motion of the reorientation of methyl groups.

As mentioned earlier, the ^{1}H-T_1 behavior at T above 50 K is analyzed by considering the magnetic dipolar interactions among proton-proton and proton-fluorine that are modulated by the reorientational motion of symmetric groups such as CH_3 and PF_6. Initially, the T_1 data analysis has been tried with this model by assuming only one type of CH_3 group, and the fit was not satisfactory. Since the system is a disordered one, all of the CH_3 groups may not in an energetically equivalent environment. In the next step, the same model has been tried by considering two inequivalent CH_3 groups: (i) CH_3 groups close to PF_6, (i.e., CH_3-1) and (ii) CH_3 groups away from PF_6,

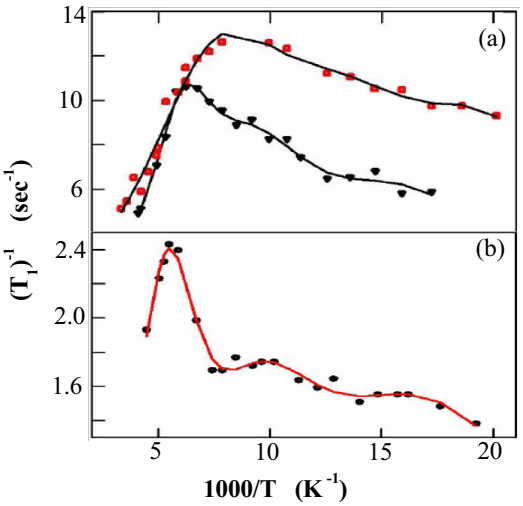

FIG. 6. (Color online) BPP model fit to (a) ^{1}H1/T_1 as a function of T for p3MT-1 (▼) and p3MT-2 (◘) at 0.9 T, (b) p3MT-1 (•) at 9 T. The solid lines are a fit to Eq. (2).

(i.e., CH_3-2) with their corresponding activation energies (E_{HH1} and E_{HH2}) and correlation times (τ_{HH1} and τ_{HH2}), along with a common correlation times (τ_{HF}) for ^{1}H and ^{19}F cross relaxation with an activation energy (E_{HF}) for PF_6 reorientation. The corresponding rate equation for the modified BPP model is given by [13,18,30,32–34]

$$\begin{aligned}\frac{1}{T_{1H}} &= C_{HH1}[J(\tau_{HH1},\omega_{HH1}) + 4J(\tau_{HH1},2\omega_{HH1})] \\ &+ C_{HH2}[J(\tau_{HH2},\omega_{HH2}) + 2J(\tau_{HH2},2\omega_{HH2})] \\ &+ C_{HF}\{J[\tau_{HF},(\omega_H - \omega_F)] + 3J(\tau_{HF},\omega_H) \\ &+ 6J[\tau_{HF},(\omega_H + \omega_F)]\} \end{aligned} \quad (2)$$

where C's are the interaction constant, $J(\tau_i,\omega_N) = \frac{\tau_i}{1+(\omega_N\tau_i)^2}$, and correlation time τ_i is $\tau_i = \tau_{i0}e^{E_i/k_BT}$.The least-squares fit has been carried out by using MATLAB.

The motional parameters from the best fit to the modified BPP model for ^{1}H-T_1 are compiled in Table II. The motion induced relaxation mechanism of the ^{1}H nuclei can be inferred from the shift of the position of the T_1^{-1} maximum to higher temperature at a Larmor frequency of 383 MHz compared to the position at 38.3 MHz. The predicted curve for 9.0 T ^{1}H-T_1^{-1} by using the fit parameters of 0.9 T ^{1}H-T_1^{-1} for p3MET-1 gives similar features with the measured parameters, which is a sign of consistent description by the BPP model. However, the measured relaxation ^{1}H-T_1^{-1} data are almost a factor of 1.3 higher than the predicted data by the fit parameters obtained at 38.3 MHz. This deviation from the BPP model hints that,with increasing Larmor frequency, the contribution of the reorientational motion to the intensity of the spectral density function decreases. Nevertheless the position of the maximum can be correctly predicted by the modified BPP model which gives the credit to the relevant fit parameters.

Our observation above, at lower frequencies, shows a reorientational motion of the CH_3 groups which is unnoticed at higher Larmor frequencies, similar to the ones studied by Mizoguchi *et al.* [30] who have carried out experiments of T_1^{-1} vs temperature as well as frequency dependence studies in FSO_3-doped PA (10^5 S/cm). They have done the experiments at considerably low NMR frequencies and over a wide temperature range. Their T_1 analysis with frequency shows q1D behavior at high frequencies and at low temperatures, while the fit deviates at lower frequencies and high temperatures. These results also suggest that at high temperature and low frequency, the sample behaves like a 3D system. Their interpretation was that the observed T_1^{-1} maximum at the high-temperature region may be due to molecular motion of FSO_3 groups, the residual moisture, and/or other reorienting groups.

Nechtschein *et al.* [14] have also shown the frequency dependence of T_1 in doped and undoped polyacetylene (PA). They observed the q1D nature in both the PAs throughout the temperature range of study, except at very low temperatures. They also concluded that at low frequency, the 1D diffusion breaks down because of interchain hopping and 2D or 3D behavior is expected. The crossover between 1D and 2D

TABLE II. Fit parameters fit to Eq. (2).

	P3MT-1			P3MT-2	
Parameters	^{19}F (9.0 T)	^{1}H (9.0 T)	^{1}H (0.9 T)	^{19}F (9.0 T)	^{1}H (0.9 T)
τ_{ii01} ($\times10^{-12}$ s)	1.63	0.18	0.639	7.54	1.38
τ_{ii02} ($\times10^{-11}$ s)	4.71	14.2	34.3	0.406	6.01
τ_{ij0}($\times10^{-11}$ s)	1.53	0.213	18.54	1.06	0.752
E_{ii1} (meV)	62.49	80.28	84.62	23.43	32.98
E_{ii2} (meV)	33.416	23.82	40.967	44.967	21.525
E_{ij}(meV)	26.038	27.51	19.529	24.389	42.92
K_{ii1} ($\times10^9$ s^{-2})	1.94	2.68	0.992	3.55	1.69
K_{ii2} ($\times10^9$ s^{-2})	3.66	2.15	0.937	3.08	1.269
K_{ij}($\times10^8$ s^{-2})	11.16	3.2	1.59	3.15	1.346
τ_{ii1} ($\times10^{-10}$ s)[a]	22.7	19.89	116.8	1.147	0.632
τ_{ii2} ($\times10^{-9}$ s)[a]	2.26	2.25	39.6	0.724	0.729
τ_{ij} ($\times10^{-10}$ s)[a]	3.13	0.517	17.8	1.79	6.9

[a]τ_{ij} and τ_{iin} are calculated at 100 K, using the relation $\tau_{iin} = \tau_{iio} \times e^{E_{iin}/k_BT}$. Subscripts i and j are the NMR nuclei.

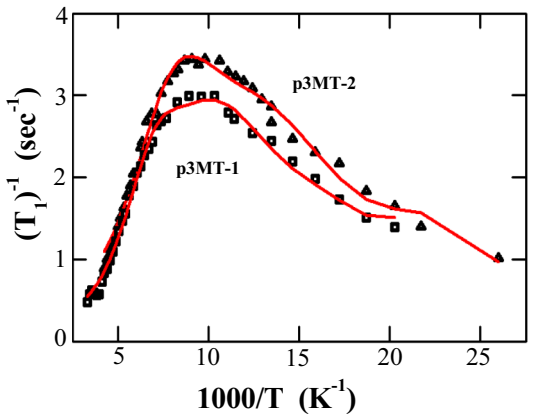

FIG. 7. (Color online) BPP model fit to ^{19}F$1/T_1$ as a function of T for p3MT-1 (■) and p3MT-2 (▲) at 9.0 T. The solid lines are fit to Eq. (2).

(or 3D) regimes is expected to occur when the interchain hopping frequency is of the same order of magnitude as the Larmor frequency. Their analysis further showed that the intrachain diffusion follows power law behavior, T^n ($n = 0.65$ above 50 K and $n = 1.5$ below 50 K). A similar trend of change of dimensionality has been noticed by Sachs *et al.* [29]. Their ^{1}H$-T_1$ studies at 293 K in organic conductors $(FA)_2PF_6$ show the relaxation is evidence of 1D diffusive motion. At low frequency the 1D model diverges. They concluded that lattice imperfections are known to spoil the one-dimensionality of the sample.

(b) ^{19}F-T_1 *studies.* Figure 7 shows T_1^{-1} for ^{19}F at 9.0 T as a function of T above 40 K for p3MT-1 and p3MT-2. The main sources for the ^{19}F relaxation are the fluctuating magnetic fields associated with the rotational motion of the PF_6 groups. Because the hyperfine field of the conduction electrons at the ^{19}F sites is expected to be weak this contribution will not be considered further. In detail, the relaxation mechanisms for ^{19}F are (i) the ^{19}F-^{19}F interaction within the same PF_6 groups, (ii) the ^{19}F-^{19}F interactions between different PF_6 groups, (iii) the magnetic dipole interaction between ^{19}F and ^{1}H nuclei, (iv) the magnetic dipole interaction between the ^{19}F and ^{31}P nuclei, and (v) contribution from chemical shield anisotropy (CSA) of PF_6. Since the interaction constants are inversely proportional to r^6 (where r is the internuclear distance) and different PF_6 groups are well separated, the contribution to T_1 from the ^{19}F$-^{19}$F interactions between different PF_6 groups is small enough and this term is left out in the following analysis. Also, because the ratio of the Larmor frequencies of ^{31}P to ^{19}F is ~ 0.432, the ^{31}P to ^{19}F cross relaxation is not expected to play a significant role in the ^{19}F relaxation process [35].

An estimate of the contribution to T_1 from chemical shield anisotropy ($\Delta\sigma$) of PF_6 groups is carried out. In samples containing fluorine nuclei, CSA may contribute to the relaxation depending on whether PF_6 is acting as a counterion strongly or weakly interacting with the polymer chains. The ^{19}F linewidth normalized absorption spectra for both samples p3MT-1 and p3MT-2 at various temperatures (figure not shown) have been used to estimate the full width at half maximum (FWHM). FWHM for both samples p3MT-1 and p3MT-2 varies from 30 kHz at 250 K to a maximum of 70 kHz at 2.78 K.Our T_1 analysis including the CSA contribution (along with reorientational motion of symmetric groups) to the relaxation mechanism shows a preexponential factor (τ_{CSA0}) $= 1.35 \times 10^{-9}$ s and activation energy (E_{CSA}) $= 146$ meV. The corresponding CSA ($\Delta\sigma$) is $\Delta\sigma = 225$ ppm which is comparable to the reported values in similar systems. With these fit parameter values, the CSA contribution (at 250 K) to $T_{1\text{total}}^{-1}$ is about 10^{-6} s^{-1}, which is quite small compared to the contribution from dipolar interaction modulated by the reorientational mechanism. Hence the ^{19}F CSA contribution has not been considered for ^{19}F, T_1^{-1} analysis.

On the other hand, the Larmor frequency of hydrogen nuclei is 1.063 times higher than that of fluorine nuclei. This shows that the cross relaxation between fluorine and hydrogen nuclei also plays a prominent role in T_1^{-1} for ^{19}F at T above 40 K. Thus the ^{19}F relaxation mechanisms are mainly due to the magnetic dipole-dipole interactions modulated by (i) the random reorientations of PF_6 and (ii) isotropic reorientations of CH_3 groups. Under these circumstances, T_1^{-1} for ^{19}F will follow the same modified BPP model described by Eq. (2), where the subscript H changes to F and F changes to H.

The motional parameters from the best fit to the modified BPP model, for both ^{19}F-T_1 and ^{1}H-T_1, are compiled in Table II. The analysis of ^{19}F and ^{1}H relaxation data obtained using this model suggests the following: Since PF_6 is relatively free to reorient, the maxima are shifted to lower temperatures, and also they are broader due to the role of interchain disorder in the relaxation mechanism. Furthermore, the relaxation data for ^{19}F in both samples are nearly identical due to the less dominant role played by the conduction electrons among these samples, and the extent of interchain disorder is rather similar in both systems.

It is revealed from the above two analyses that even though PF_6 is a heavier group than CH_3, the T_1^{-1} maximum at 9.0 T in the case of ^{19}F is observed at lower temperature compared to ^{1}H at that field. This can be explained by considering the fact that the PF_6 group is relatively free to reorient as it is situated in between the chains (see Fig. 1) whereas CH_3 is attached to the polymer backbone. Thus the correlation time for PF_6 is shorter than that of CH_3; accordingly the T_1^{-1} maximum for PF_6 motion is observed at lower temperatures. It is evident from the general BPP equation that T_1 exhibits a minimum when $\omega_0\tau_c = 0.615$, and the corresponding maximum in T_1^{-1} of nuclei "i" with nuclear spin I is given by $T_{1i}^{-1} = \frac{3\times1.42\gamma_i^4\hbar^2 I(I+1)}{2r^6\omega_{oi}}$, where γ_i is the nuclear gyromagnetic ratio of nuclei i, $\bar{h}$ is the reduced Planck's constant, r is the internuclei distances, and ω_{oi} is the Larmor frequency of the nuclei i. It has been found that $T_{1H}^{-1}/T_{1F}^{-1} > 1$, from the known values of γ, ω_o, r, I, and $\bar{h}$ for ^{19}F and ^{1}H. This has been further verified from the estimated values of $\omega_{0H}\tau_{cHH}$ and $\omega_{0F}\tau_{cFF}$ at a given temperature (say 150 K), and found that τ_{cFF} is shorter than τ_{cHH} due to the facile motion of PF_6, as explained above.

Similar observation of PF_6 motion has been studied by Wieland *et al.* [31] in organic metal $(perylene)_2(AsF_6)_{0.75}(PF_6)_{0.35} \times 0.85CH_2Cl_2$. Their ^{1}H-$T_1$ studies revealed a linear dependence of T_1^{-1} against $f^{-1/2}$, showing a signature of a one-dimensional motion of the spins. T_1^{-1} against temperature in the range 300–180 K, showed a linear variation as expected of an organic metal. The observed

T_1^{-1} maximum around 50 K is ascribed to coupling to the ^{19}F spins of reorienting PF_6 groups. This also supports the view that ^{1}H relaxation shows signatures of relaxation due to one-dimensional motion of spins as well as reorienting groups depending on which process dominates at the temperature under consideration. Hoptner *et al.* [17] have carried out ^{1}H-T_1 and ^{19}F-T_1 in radical cation salt, $(\text{fluoranthenyl})_2^+PF_6^-$ as a function of temperature. They observed that ^{19}F-T_1 are relaxed mainly by the reorientational motion of the anions and by the interaction with fixed paramagnetic impurities; the protons are relaxed additionally above 150 K predominantly by highly mobile paramagnetic species, whose concentration could be determined directly via the NMR signal amplitude. These observations support our view of PF_6 reorientation motion being responsible for spin lattice relaxation. The Korringa relation observed for proton relaxation shows that it is metallic above 183 K. Further, frequency dependence of T_1 of proton relaxation supports the one-dimensional spin transport and also confirms that only protons of the cation stacks are relaxed by the highly mobile paramagnetic species.

4. Relaxation mechanism dominated by spin diffusion to paramagnetic centers (SDPC) and the modified Korringa relation

As the temperature decreases, the relaxation due to the reorientation motions of the symmetric groups slows down and freezes at a particular temperature. Once the temperature is low enough, the main contribution to the relaxation mechanism is due to the SDPC process and the motion of charge carriers. A drawing of the SDPC process is shown in Fig. 8, where the filled black circle is the paramagnetic center, the elliptical shaped ones are the nuclear spins, the nuclei inside the shaded region are shifted in frequency so much that they do not interact with the others, the nuclei within the radii d and b are relaxed directly by the fluctuating magnetic field generated by exchanging magnetization to the paramagnetic center (frozen electrons), and those outside the radius b are relaxed by nuclear spin diffusion. In the spin diffusion process, the spins closer to the paramagnetic center recover more quickly than those farther away. But after a long enough time, all of them reach an equilibrium spin temperature. These types of relaxation mechanisms have been reported in other systems [1,36–38].

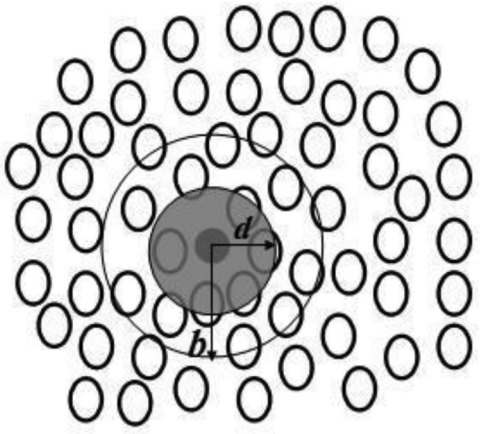

FIG. 8. Drawing of the SDPC process. (•) paramagnetic center. 0 is nuclear spins. The d region is the region of frequency shifted nuclei. $b - d$ is the region of nuclei that directly relaxed to the paramagnetic center. Nuclei outside the region b are relaxed by nuclear spin diffusion.

It is interesting to recall that as the temperature decreases, T_1 behavior is more and more towards 3D. Since the protons are in the polymer backbone thus their relaxation may be mainly due to both intra- and interchain hopping of the charge carriers.

At temperatures below 50 K, T_1^{-1} is proportional to temperature as shown in Fig. 9. This follows the modified

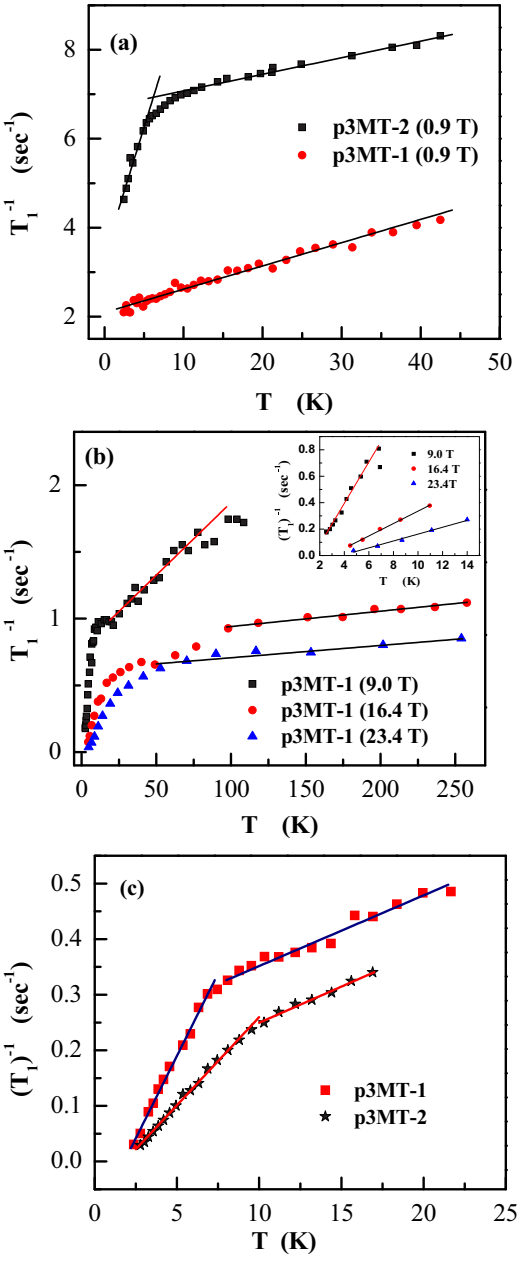

FIG. 9. (Color online) (a) ^{1}H-T_1 dependence of temperature at 0.9 T. Solid line is fit to the modified Korringa relation expressed by Eq. (3). (b) ^{1}H-T_1 dependence of temperature of p3MT-1 at various fields. Inset: ^{1}H-T_1 as a function of temperature, $T < T_Z$. Solid line is fit to the modified Korringa relation expressed by Eq. (3). (c) ^{19}F-T_1 dependence of temperature at 9.0 T. Solid line is fit to the modified Korringa relation expressed by Eq. (3).

Korringa relation, as reported earlier in PPy-PF_6. The analysis of T_1 data using the modified Korringa relation [11,39] takes into account the contributions due to disorder, and EEI [3,12,17,40–44] is expressed as [3,13,17,44]

$$K^2 T_1 T \left(1 + \frac{\varepsilon}{2}\right) C_o S_K = 1. \quad (3)$$

Here $C_0 = (\gamma_n/\gamma_e)^2 (4\pi k_B/\hbar)$; ε(=Knight shift anisotropy $= d^2/a^2$) is the ratio of the anisotropic and isotropic contributions to the hyperfine interaction [3], which plays an important role in the relaxation of organic materials; S_K is the Korringa enhancement factor which includes the role of EEI along with disorder. The Korringa enhancement factor contains the spectral density of interaction and is expressed as

$$S_K = \frac{1}{2}\left(\frac{\tau_\perp}{\tau_s}\right)^{1/2} \left[\frac{3}{5}\varepsilon J(\omega_n) + \left(1 + \frac{7}{5}\varepsilon\right) J(\omega_e)\right] K_o(\alpha) + \frac{1}{2}(1 + 2\varepsilon) K_{2k_F}(\alpha). \quad (4)$$

The quantity $\varepsilon(=d^2/a^2)$ is the ratio of anisotropic to isotropic contribution of the hyperfine interaction and $J(\omega) = [(1 + \omega^2\tau_\perp^2)^{1/2} + 1]/[2(1 + \omega^2\tau_\perp^2)]$ is the spectral density of interaction with ω_e and ω_n being the electron and nuclear precession frequencies, respectively. In addition to this, $K_o(\alpha)$ and $K_{2kF}(\alpha)$ are given by the expressions $K_o(\alpha) = (1 - \alpha)^{1/2}$ and $K_{2kF}(\alpha) = (1 - \alpha)^2/[1 - \alpha F(2k_F)]$ [2]; $F(2k_F) = (1/2)[\ln(4.56T_F/T)]$, the Lindhart function; T_F is the Fermi temperature. In this expression $\tau_\perp$ is the interchain hopping time, τ_s is the phonon scattering time along the chain, and α is the interaction parameter. For classical metals, $\varepsilon = 0$ and $S_K = 1$, and the Korringa relation is recovered. In organic conductors, for example, fluoranthene-PF_6, with highly anisotropic conduction, S_K has values from 50 to 500, and $0 < \varepsilon < 4$, showing a large deviation from that of a classical metal [45].

The fits for ^{1}H-T_1 data to Eq. (3) yield straight lines, though the lines do not pass through the origin, as shown in Figs. 9(a)–9(c). In conventional Korringa behavior the fit is supposed to pass through the origin, unlike the present case. The change in slopes is related to the change in Knight shift which in turn is related to the EEI and disorder. An important feature of these fits is the following: (1) It shows a positive intercept, which implies a finite relaxation time at $T \to 0$ K, and this is attributed to the EEI contribution to the relaxation mechanism; and (2) the rapid decrease in the positive intercept implies that the relaxation mechanism is becoming considerably weak as $T \to 0$ K. The value of S_K from the fit to Eq. (3) is shown in Table III. The ^{1}H-T_1 data for $T < 50$ K and at 0.9 T is shown in Fig. 9(a).

The change in slope is observed only in the case of p3MT-2; since the number of conduction electrons is less, the relaxation process has slowed down considerably, unlike in the case of p3MT-1. One of the important reasons to carry out high-field T_1 measurement is that at the particular temperature below the value given by $T_Z = g\mu_B B/2k_B$, the local electron moment magnetization saturates, and this eliminates the contribution from SDPC to the relaxation mechanism; this in turn makes a Korringa-like process as the dominant relaxation mechanism [20,36,46,47]. Hence it is quite reasonable to use the modified Korringa relation to explain the low-temperature $(T < T_Z)\,T_1$ data. At $T > T_Z$, the fits to Eq. (3) yield the values of S_K (see Table III) in the range of 1–15, which is quite reasonable.

TABLE III. S_K values at different fields and temperatures.

Samples	Field	S_K values	
		S_{K1} $(T > T_Z)$	S_{K2} $(T < T_Z)$
p3MT-1	0.9 T (^{1}H)	68.86	
	9.0 T (^{1}H)	14.33	205
	9.0 T (^{19}F)	18.91	88.05
	16.4 T (^{1}H)	1.514	61.75
	23.4 T (^{1}H)	1.211	34.16
p3MT-2	0.9 T (^{1}H)	49.11	755.76[a]
	9.0 T (^{19}F)	19.31	47.07

[a] $T < 6$ K, not $T < T_Z$.

Interestingly, in p3MT-2 an increase in slope in ^{1}H-T_1 at 0.9 T is observed below 6 K, while in p3MT-1 it is not observed till 2.5 K. This is due to the fact that in p3MT-2 the number of conduction electrons is less than that in p3MT-1, and this increases the interaction among the localized spins, resulting in a freeze-out of spin diffusion to paramagnetic centers (SDPCs) at higher temperature.

In the case of ^{19}F (at 9 T) the increase in T_1 occurs at the same temperature for both p3MT-1 and p3MT-2. However, the S_K values for $T < T_Z$, as shown in the inset of Fig. 9(b), are rather large (34–205), indicating deviations from the Korringa relation. Furthermore, the S_K values vary inversely with field, suggesting that the field-induced localization of carriers is reducing the contribution arising from EEI to S_K. Also the S_K values (∼19) for ^{19}F-T_1 data at $T > T_Z$, as in Fig. 9(c), are similar to those observed in ^{1}H-T_1 data; at $T < T_Z$ the data show deviation. The S_K value for p3MT-1 is higher than that in p3MT-2, since the contributions from both EEI and disorder are larger in the former case. Hence both the ^{1}H-T_1 and ^{19}F-T_1 data consistently show that the role of EEI is quite significant in the values of S_K and the relaxation mechanism at low temperatures. Nevertheless these large values for S_K at low temperatures indicate that the model [as in Eq. (3)] is not fully satisfactory to take into account the roles of both disorder and EEI.

From the above analysis (Secs. III C 3a and III C 4), we can explain the observation of a faster relaxation rate of ^{1}H (below 150 K) in p3MT-1 than for p3MT-2 (item 2 in Sec. III B) as follows. Above 50 K the relaxation is due to the reorientation of the symmetric subgroups. In conducting polymers, the rigidity of the chains increases at higher doping level and this restricts the degrees of freedom for the reorienting groups. Also, the presence of a larger number of dopants in p3MT-1 hinders the reorientation of the CH_3 groups as the potential barriers increase. This results in a decrease of $1/T_1$, provided that τ_c for the CH_3 rotation decreases due to the increase in the potential barrier corresponding to the increased number of PF_6 groups.

Further below 50 K, the reorientational motions of symmetric groups like CH_3 and PF_6 tend to freeze. However, a finite relaxation time has been observed below 50 K, indicating the possibility for other mechanisms, and this is largely due to the relaxation via the conduction electrons. Here the fluorines are relaxed via spin diffusion to the methyl group protons, which in turn are relaxed to the lattice via conduction electrons. Since more PF_6 is present in p3MT-1, more fluorines relax via spin diffusion to protons, hence the $1/T_1$ in p3MT-1 is less than that in p3MT-2.

Combining the analysis of Secs. III C 3b and III C 4, one can explain the observation of crossover in ^{19}F-T_1^{-1} between p3MT-1 and p3MT-2 (item 5 in Sec. III B). Although the reorientational motion of PF_6 groups is the dominant relaxation mechanism at higher temperatures in both samples, the PF_6 groups in p3MT-2 are relatively free to reorient, since the chains in p3MT-1 are more rigid, as discussed before. However, below $T < 25$ K the relaxation of fluorine via the methyl protons to the conduction electrons seems to occur faster in p3MT-1 due to the availability of a larger number of conduction electrons compared to p3MT-2; this mechanism becomes more relevant when the activated reorientational motions are frozen.

A comparison of the ^{19}F-T_1^{-1} and ^{1}H-T_1^{-1} can give an insight into the interchain and intrachain relaxation mechanisms. Since PF_6 is sandwiched between the polymer chains, the ^{19}F nuclei thus can relax on either side of the polymer chain. However, the ^{1}H relaxation mechanism can occur mainly along the chain, as protons are attached to the polymer backbone.

The ^{19}F-T_1^{-1} data in Fig. 4(b) show the crossover between p3MT-1 and p3MT-2 samples at $T \sim 25$ K. However, such a crossover has not been observed in the ^{1}H-T_1^{-1} measurements. These data indicate that a systematic investigation of both the ^{1}H and ^{19}F relaxation mechanisms can probe the interchain vs intrachain relaxation mechanism. However, these results warrant more detailed investigation in the future. Thus the analysis of relaxation time in p3MT samples shows that ^{1}H-T_1 can be a good probe to monitor the intrachain mechanism while ^{19}F-T_1 (NMR nuclei in the dopant) can probe the interchain processes.

It is interesting to discuss the T_1 data at 9.0, 16.3, and 23.4 T below T_Z. $(T_1T)^{-1}$ vs T data [Figs. 4(c) and 4(d)] at these fields show pinning of paramagnetic centers at 0.6, 6.04, 11.02, and 15.72 K for 0.9, 9.0, 16.4, and 23.4 T, respectively. Hence, a modified Korringa relation with EEI and disorder will dominate the relaxation mechanism with a positive slope below the corresponding temperatures, while above these temperatures a modified Korringa relation with SDPC, EEI, and disorder with a negative slope will be the relaxation mechanism up to the highest temperature of experiment.

As discussed in the Experimental Details section, from the equilibrium amplitudes of the proton and fluorine FID signals, it was found that the dopant concentration in p3MT-1 is two orders of magnitude higher than that from p3MT-2. The dc conductivity data also have shown that p3MT-1 has higher conductivity than p3MT-2. The $N(E_F)$ calculation from susceptibility data also shows that its value in p3MT-1 is two orders higher than p3MT-2. This shows that there is an internal consistency in the data analysis.

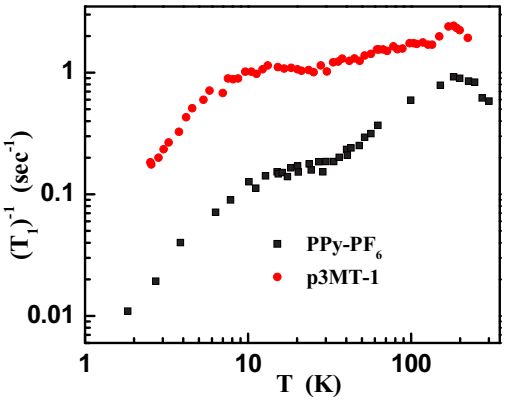

FIG. 10. (Color online) Comparison of ^{1}H$-T_1$ between metallic PPy-PF_6 and p3MT-1.

D. Comparison with the metallic PPy-PF_6

It is interesting to compare the results in p3MT with similar studies [13] in metallic PPy-PF_6. In the latter, the relaxation below 6 K follows a modified Korringa relation, while at intermediate temperature ($6 < T < 50$ K) and high temperature ($T > 50$ K) the relaxation is due to SDPC and reorientation of PF_6 groups, respectively. One of the important differences between the two systems is that the conductivity of pPy-PF_6 is large ($\sim$150 S/cm) even at 20 mK, while in fully doped p3MT-1 the conductivity changes by two orders of magnitude from room temperature down to 77 K, and at very low temperature the conductivity is quite low as in typical insulators. Proton and fluorine T_1 measurements show some common features: (i) reorientation of PF_6 groups; (ii) SDPC followed by modified Korringa relation, as shown in Fig. 10. In pPy-PF_6 the protons, that are bound to the main chain, are relaxed due to the reorientation of PF_6 groups; while in p3MT-1 the proton relaxation is due to both CH_3 and PF_6 groups. The main difference is that the enhancement factor in S_K in p3MT samples at low temperature is quite high, which shows a large deviation from the Korringa relation, unlike in metallic pPy-PF_6 films.

The present study also shows the crossover in ^{19}F relaxation as a function of temperature in doped and dedoped samples. This indicates that ^{19}F (NMR nuclei in the dopant) T_1^{-1} measurements can be used to probe the interchain conduction mechanism, while ^{1}H probes the intrachain conduction mechanism.

IV. CONCLUSIONS

Conductivity, magnetic susceptibility, and NMR T_1 (proton and fluorine) measurements have been carried out in both fully doped and dedoped p3MT samples. Conductivity of both p3MT samples decreases by two orders of magnitude at 77 K. Magnetic susceptibility data show the presence of both Curie and Pauli spins. The number of Pauli spins in p3MT-1 is two orders of magnitude larger than that in p3MT-2. Measurements of proton and fluorine NMR T_1 show that the reorientation of the symmetric subgroups like CH_3 and PF_6 is the dominant relaxation mechanism at low frequency and higher temperatures. Three different types of relaxation mechanism have been identified in these systems.

Relaxation at high temperatures is due to the reorientation of symmetric subgroups. In the intermediate temperature region, the relaxation mechanism is dominated by the SDPC followed by modified Korringa relaxation and at very low temperature ranges deviations from Korringa-like relaxation is observed. Present high-field and low-temperature measurements show that relaxation through paramagnetic centers can be pinned at any given temperature depending on the magnitude of the field. Further, this work clearly signifies that the same system can show different dimensionality depending upon the window (temperature and frequency) of observation.

ACKNOWLEDGMENTS

The authors thank DST-NSF for financial assistance to carry out this work. The work at Los Alamos was performed under the auspices of the U.S. Department of Energy, Office of Science. The work done by the UCLA authors was supported by NSF Grants No. DMR-0334689 and No. OISE-0225578. The work at the NHMFL Tallahassee received the financial support from the National Science Foundation under cooperative agreement No. DMR-0084173 and the State of Florida.

[1] N. Bloembergen, Physica **15**, 588 (1949).
[2] G. Sachs and E. Dormann, Synth. Met. **25**, 157 (1988).
[3] A. C. Kolbert, S. Caldarelli, K. F. Their, N. S. Sariciftci, Y. Cao, and A. J. Heeger, Phys. Rev. B **51**, 1541 (1995).
[4] L. K. Alexander, N. Büttgen, R. Nath, A. V. Mahajan, and A. Loidl, Phys. Rev. B **76**, 064429 (2007).
[5] A. Narath and D. C. Barham, Phys. Rev. **176**, 479 (1968).
[6] J. Szeftel and H. Alloul, J. Non-Cryst. Solids **29**, 253 (1978).
[7] T. L. Reinecke and K. L. Ngai, Phys. Rev. B **12**, 3476 (1975).
[8] A. Avogadro, F. Tabak, M. Corti, and F. Borsa, Phys. Rev. B **41**, 6137 (1990).
[9] P. W. Anderson, B. I. Halperin, and C. M. Varma, Philos. Mag. **25**, 1 (1972).
[10] W. A. Phillips, J. Low Temp. Phys. **7**, 351 (1972).
[11] J. Korringa, Physica **16**, 601 (1950).
[12] B. S. Shastry and E. Abrahams, Phys. Rev. Lett. **72**, 1933 (1994).
[13] K. J. Singh, W. G. Clark, K. P. Ramesh, and M. Reghu, J. Phys.: Condens. Matter **20**, 465208 (2008).
[14] M. Nechtschein, F. Devreux, R. L. Greene, T. C. Clark, and G. B. Street, Phys. Rev. Lett. **44**, 356 (1980).
[15] K. Mizoguchi and K. Kume, Solid State Commun. **89**, 971 (1994).
[16] G. Soda, D. Jerome, M. Weger, J. M. Fabre, and L. Giral, Solid State Commun. **18**, 1417 (1976).
[17] W. Hoptner, M. Mehring, J. U. Von Schutz, H. C. Wolf, B. S. Mora, V. Enkelmann, and G. Wegner, Chem. Phys. **73**, 253 (1982).
[18] A. Kaiser, B. Pongs, G. Fischer, and E. Dormann, Phys. Lett. A **282**, 125 (2001).
[19] S. Masubuchi, T. Fukuhara, and S. Kazama, Synth. Met. **84**, 601 (1997).
[20] M. Nechtschein, in *Handbook of Conducting Polymers*, 2nd ed., edited by T. A. Skotheim, R. L. Eisenbaumer, and J. R. Reynolds (Marcel Dekker, New York, 1998), p. 141.
[21] R. Menon, in *Handbook of Conducting Organic Conductive Molecules and Polymer*, edited by H. S. Nalwa (Wiley, New York, 1997), Vol. 4, p. 47.
[22] N. S. Sariciftci, A. J. Heeger, and Y. Cao, Phys. Rev. B **49**, 5988 (1994).
[23] Y. Long, Z. Chen, J. Shen, Z. Zhang, L. Zhang, H. Xiao, M. Wan, and J. L. Duvail, J. Phys. Chem. B **110**, 23228 (2006).
[24] H. S. Nalwa, J. Polym. Sci., Part C: Polym. Lett. **26**, 351 (1988).
[25] P. K. Kahol, Phys. Rev. B **62**, 13803 (2000).
[26] P. K. Kahol, J. C. Ho, Y. Y. Chen, C. R. Wang, S. Neeleshwar, C. B. Tsai, and B. Wessling, Synth. Met. **151**, 65 (2005).
[27] F. Moraes, D. Davidov, M. Kobayashi, T. C. Chung, J. Chen, A. J. Heeger, and F. Wudl, Synth. Met. **10**, 169 (1985).
[28] R. S. Kohlman, J. Joo, and A. J. Epstein, in *Physical Properties of Polymers Handbook*, edited by J. E. Mark (AIP Press, New York, 1996), p. 459.
[29] G. Sachs, E. Dormann, and M. Schwoerer, Solid State Commun. **53**, 73 (1985).
[30] K. Mizoguchi, F. Shimizu, and K. Kume, Synth. Met. **41**, 185 (1991).
[31] J. Wieland, U. Haeberlen, D. Schweitzer, and H. J. Keller, Synth. Met. **19**, 393 (1987).
[32] B. Bloembergen, N. Purcell, and R. V. Pound, Phys. Rev. **73**, 679 (1948).
[33] G. Nemec, V. Illich, and E. Dorman, Synth. Met. **95**, 149 (1998).
[34] C. H. Tso, J. D. Madden, and C. A. Michal, Synth. Met. **157**, 460 (2007).
[35] E. C. Reynhardt, S. Jurga, and K. Jurga, Chem. Phys. Lett. **194**, 410 (1992).
[36] A. Abragam, *Principles of Nuclear Magnetism* (Oxford University Press, Oxford, 1961).
[37] N. Bloembergen, Physica **15**, 386 (1949).
[38] M. Sutirtha, K. P. Ramesh, R. Kannan, and J. Ramakrisna, Phys. Rev. B **70**, 224202 (2004).
[39] C. P. Slichter, in *Principles of Magnetic Resonance*, 3rd ed. (Springer, Heidelberg, 1989), p. 156.
[40] A. Narath and H. T. Weaver, Phys. Rev. **175**, 373 (1968).
[41] W. S. Robert, Jr. and W. W. Warren, Jr., Phys. Rev. B **3**, 1562 (1971).
[42] G. Soda, D. Jerome, M. Weger, J. Alizon, J. Gallice, H. Robert, J. M. Fabre, and L. Giral, J. Phys. (Paris) **38**, 931 (1977).
[43] K. F. Their, C. Goze, M. Mehring, F. Rachdi, T. Yildrim, and J. E. Fischer, Phys. Rev. B **59**, 10536 (1999).
[44] M. Mehring, in *Low Dimensional Conductors and Superconductors*, edited by D. Jerome and L. S. Caron (Plenum Press, New York, 1987), p. 185.
[45] D. Köngeter and M. Mehring, Phys. Rev. B **39**, 6361 (1989).
[46] E. R. Andrew, in *Nuclear Magnetic Resonance* (Cambridge University Press, Cambridge, 1955), p. 192.
[47] W. G. Clark, K. Tanaka, S. E. Brown, R. Menon, F. Wudl, W. G. Moulton, and P. Kuhns, Synth. Met. **101**, 343 (1999).